Article

Current Biology

Repulsion of hippocampal representations driven by distinct internal beliefs

Highlights

- Spatial-route overlap induces repulsion of activity patterns in CA3 and dentate gyrus
- Repulsion depends on visual input being similar while internal beliefs are distinct
- Even when visual input is identical, repulsion can occur by manipulating beliefs
- Repulsion cannot be explained by standard accounts of pattern separation

Authors

Guo Wanjia, Subin Han, Brice A. Kuhl

Correspondence

wanjiag@uoregon.edu (G.W.),
bkuhl@uoregon.edu (B.A.K.)

In brief

Wanjia et al. show that representations of overlapping spatial routes in human CA3 and dentate gyrus are dramatically differentiated when visual similarity between the routes is high—or even identical—but internal beliefs are distinct. These findings are not accounted for by standard models of pattern separation in the hippocampus.

Wanjia et al., 2025, Current Biology *35*, 2893–2902
June 23, 2025
https://doi.org/10.1016/j.cub.2025.05.029

CellPress

Current Biology

CellPress
OPEN ACCESS

Article

Repulsion of hippocampal representations driven by distinct internal beliefs

Guo Wanjia,[1,2,*] Subin Han,[3] and Brice A. Kuhl[1,2,4,*]
[1]Department of Psychology, University of Oregon, 1451 Onyx St., Eugene, OR 97403, USA
[2]Institute of Neuroscience, University of Oregon, 1585 E 13th Ave., Eugene, OR 97403, USA
[3]Department of Psychology, University of Virginia, Gilmer Hall, 485 McCormick Rd., Charlottesville, VA 22904, USA
[4]Lead contact
*Correspondence: wanjiag@uoregon.edu (G.W.), bkuhl@uoregon.edu (B.A.K.)
https://doi.org/10.1016/j.cub.2025.05.029

SUMMARY

Recent human neuroimaging studies of episodic memory have revealed a counterintuitive phenomenon in the hippocampus: when events are highly similar, corresponding hippocampal activity patterns are sometimes less correlated than activity patterns associated with unrelated events. This phenomenon—*repulsion*—is not accounted for by most theories of the hippocampus, and the conditions that trigger repulsion remain poorly understood. Here, we used a spatial route-learning task and high-resolution fMRI in humans to test whether hippocampal repulsion is fundamentally driven by internal beliefs about the environment. By precisely measuring participants' internal beliefs and actively manipulating them, we show that repulsion selectively occurred in hippocampal subfields CA3 and dentate gyrus when visual input was ambiguous—or even *identical*—but internal beliefs were distinct. These findings firmly establish conditions that elicit repulsion and have broad relevance to theories of hippocampal function and to the fields of human episodic memory and rodent spatial navigation.

INTRODUCTION

Central to the hippocampus' role in episodic memory is its capacity to encode highly overlapping events while limiting potential interference.[1–5] Recent human neuroimaging studies have identified a surprising way in which the hippocampus supports this goal: by inverting the representational structure of visual stimuli. That is, the hippocampus will—at least in some situations—form representations of overlapping events that are *less similar* (i.e., less correlated activity patterns) than representations of completely unrelated (non-overlapping) events.[6–14] This phenomenon has been termed *repulsion* because representations of overlapping events appear to "move away" from each other. While this phenomenon has been observed several times, it is not entirely clear when or why repulsion occurs. Understanding the circumstances that elicit repulsion is of broad relevance to theories of memory and spatial navigation—both in humans and rodents—as leading theoretical accounts of the hippocampus largely fail to address or explain this surprising phenomenon.[1,3,4,15]

It is important to first note that repulsion is computationally distinct from traditional views of pattern separation.[16,17] The dominant view of pattern separation is that the hippocampus *orthogonalizes* input from sensory areas (e.g., input from the visual cortex).[1,2,18] This can be conceptualized via an input-output function where, for every unit increase in the similarity of sensory input, the increase in hippocampal similarity (output) will be relatively smaller.[2,19] With perfect orthogonalization, increases in input similarity would not increase similarity in the hippocampus at all. In other words, the ceiling for orthogonalization is a flat input-output function. By contrast, repulsion occurs if an increase in input similarity leads to a *decrease* in hippocampal similarity—i.e., a portion of the input-output function that is *negatively sloped*[13] (Figure S1).

To understand why hippocampal repulsion occurs, it is essential to understand when it occurs. While event similarity is, by definition, a necessary ingredient for repulsion, similarity does not always induce hippocampal repulsion. Indeed, there are many examples where hippocampal pattern similarity is relatively greater when events have overlapping elements.[20–23] One factor that seems to be important for inducing repulsion is the degree of experience with overlapping events. Namely, repulsion may only emerge with extensive training.[6,17] However, experience, per se, is not a satisfying explanation—rather, experience is presumably correlated with some change in behavior or memory that explains why hippocampal representations ultimately exhibit repulsion.[9]

Perhaps the most intuitive explanation is that repulsion only emerges once participants learn to visually attend to subtle differences between stimuli. However, a visual attention account predicts that effects should first emerge in visual cortical areas and only then be passed on to the hippocampus. By contrast, repulsion effects in the hippocampus have been shown to occur without any precipitating effects in the visual cortex.[6,7,9] That said, a modified version of this account could be that the hippocampus amplifies subtle differences in visual cortical areas.

An alternative account is that repulsion has less to do with differences in visual attention and more to do with differences in internal beliefs. From this perspective, the hippocampus is not inheriting or amplifying differences from the visual cortex but

is, instead, generating these differences internally. This account is motivated by recent theory[24] and evidence from studies of rodents,[25,26] which argue that changes in hippocampal activity patterns (place cell remapping) are better explained by shifts in internal (or latent) representations than by observable features of the environment. That said, it is not clear whether theories of place cell remapping in rodents apply to the phenomenon of hippocampal repulsion in human memory. Indeed, the phenomenon of repulsion has not been reported in rodent place cells (however, it has been anticipated in computational models[27]).

Here, we tested whether hippocampal repulsion occurs when internal beliefs are distinct, but visual stimuli are ambiguous. We used high-resolution fMRI and a spatial route-learning paradigm in which human participants learned pairs of overlapping routes. Inspired by classic rodent T-maze designs,[28,29] the routes initially overlapped but eventually diverged. Specifically, the overlapping routes were visually identical at first ("same segment"), then became very slightly different ("similar segment") before diverging ("different segment") and terminating at unique destinations. This allowed us to assess the similarity of fMRI activity patterns—in the hippocampus and visual cortical areas—as a function of route segment. We took two approaches to linking hippocampal activity patterns to internal beliefs. First, we obtained participant-specific measures of the time point within each route when participants were able to confidently predict a route's destination, allowing us to test whether hippocampal repulsion was temporally coupled with these "moments of insight" (MoIs). Second, we manipulated beliefs by using probabilistic cues that indicated the likely route destination. This afforded a causal test of whether distinct beliefs, in the face of ambiguous input, drive hippocampal repulsion.

We show that hippocampal subfields CA3 and dentate gyrus (CA3/DG) exhibited repulsion effects when visual input was extremely similar—or even *identical*—but internal beliefs were distinct. These findings provide insight into when and why repulsion occurs and establish the relevance of this poorly understood representational phenomenon to memory interference and spatial navigation.

RESULTS

Each participant repeatedly viewed a slideshow of images depicting four routes (2 overlapping pairs) from the University of Oregon campus. Overlapping routes started on identical paths with identical images (same segment, 6 s, 25 pictures), followed by identical paths with highly similar images (similar segment, 12 s, 50 pictures), then different paths with distinct images (different segment, 6 s, 25 pictures) (Figure 1A). Each route terminated at a unique landmark, or destination, which was identified by a text label (e.g., "pole," 2 s). Participants gained familiarity with the routes before fMRI scanning and then repeatedly viewed each route during scanning. Critically, during fMRI scanning—and only during fMRI scanning—each trial was preceded by a probabilistic cue (75% valid) indicating the likely destination. Invalid cues always indicated the destination of the overlapping route.

Behavioral results

Before, during, and after scanning, participants were tested on their ability to predict each route's destination. Prior to scanning, participants completed a pre-test in which the route slideshow paused and participants selected the route destination from all 4 possible destinations. Participants then indicated their confidence (high/low). Pauses occurred equally often during the same, similar, and different segments. We refer to the correct destination as the "target," the overlapping route's destination as the "competitor," and the other two destinations as "non-overlapping" destinations. As expected, competition between the overlapping routes was highest during the same segment, was lower but still present during the similar segment, and was fully resolved during the different segment (Figure 1C; see Table S1 for statistical comparisons).

During fMRI scanning, routes occasionally paused (25% of trials), and participants were instructed to select the correct destination. These trials were only included to promote participant engagement and vigilance, and performance on these trials is not easily interpreted because they were always preceded by a valid cue (see STAR Methods).

After fMRI scanning, participants completed two post-tests. The first post-test was similar to the pre-test except that the routes only paused during the similar segment and only the target and competitor destinations were shown (see STAR Methods). Performance markedly improved across time points within the similar segment (see Table S2).

In the second post-test, participants viewed the routes again and were instructed to press a button as soon as they were at least "90% sure" of the destination. Upon making a button press, the route paused, and participants selected the destination from the full set of 4 options. Participants selected the target on 94.84% (mean) ± 7.99% (standard deviation) of the trials. For trials on which the target was selected, the mean response time was 9.36 ± 1.96 s (relative to route onset), which corresponded to the first half of the similar segment (early-similar segment). While there was variability across participants (range: 6.99–12.77 s; Figure 1D), each participant's mean response time fell within the similar segment (which spanned 6.0–18.0 s).

fMRI pattern similarity as a function of route segment

For each participant, trial, and region of interest (ROI), we extracted each voxel's activation at each 1 s time point, excluding the cue and destination (24 time points included in total). Following prior studies,[6,7,9] we focused analyses on the hippocampus, parahippocampal place area (PPA), and early visual cortex (EVC). We specifically considered hippocampus subfields CA1 and CA3/DG (Figure 2A; for additional medial temporal lobe regions, see Figure S2). We predicted repulsion effects would be selective to CA3/DG, based on findings from related studies.[9,11,21,25]

Pattern similarity values were computed, at each time point, by correlating activity patterns from different routes across different scan runs. Correlations between non-overlapping routes were subtracted from correlations between overlapping routes, yielding a "similarity score" (for an alternative approach, see Figure S3). Positive similarity scores indicate that overlapping routes were more similar than non-overlapping routes. Negative similarity scores indicate that overlapping routes were less similar than non-overlapping routes (repulsion). It is important to emphasize that overlapping and non-overlapping routes do not refer to different *routes*[30] but to different

CellPress
OPEN ACCESS

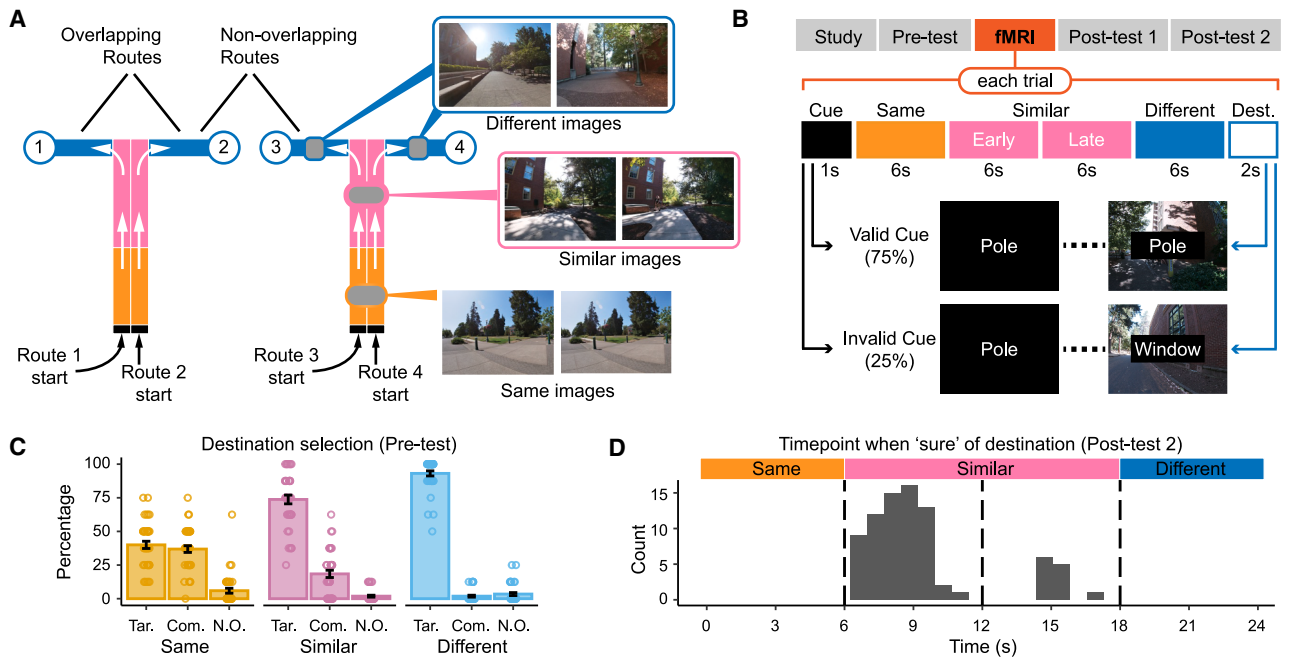

Figure 1. Experimental paradigm and behavioral results

(A) Schematic illustration of overlapping and non-overlapping routes. Each participant studied two pairs of overlapping routes. Overlapping routes (e.g., routes 1 and 2) initially followed identical paths with identical images (same segment, orange) before continuing on identical paths with subtly different images (similar segment, pink) and then diverging on different paths with different images (different segment, blue) to terminate at unique destinations (circles). For non-overlapping routes (e.g., routes 1 and 3), paths and images were always distinct.

(B) Overview of experimental phases and fMRI trials. During the fMRI phase, each trial was preceded by a cue (1 s) indicating the likely destination (75% valid; 25% invalid). Invalid cues always referred to the overlapping route's destination. The cue was followed by a stream of 100 images displayed across 24 s (same segment = 6 s; similar segment = 12 s; different segment = 6 s). The destination was then displayed for 2 s.

(C) During the pre-test, routes paused during each segment, and participants were instructed to choose the correct destination. Within the same segment, participants were equally likely to choose the target (Tar.) or competitor destination (Com.). Within the similar segment, the target was selected more often than the competitor, and the competitor more often than a non-overlapping destination (N.O.). Within the different segment, participants overwhelmingly selected the target. Error bars are SEM. See Table S1 for additional pre-test data and statistical analyses.

(D) In post-test 2, participants viewed routes (without destination cues) and were instructed to press a button when they were 90% sure of the destination. The histogram shows the distribution of responses across time. See Table S2 for additional post-test data and statistical analyses.

comparisons between routes. For example, routes 1 and 2 were overlapping routes, but routes 2 and 3 were non-overlapping routes (Figure 1A). For initial analyses, we only included trials preceded by valid destination cues, and we divided each route into four evenly spaced segments (6 s each): same, early-similar, late-similar, and different. While overlapping routes were not discriminable based on visual information during the same segment, the valid destination cues allowed participants to "believe" that the routes were distinct even during the same segment.

A two-way ANOVA with factors of segment and ROI (CA3/DG, CA1, PPA, and EVC) revealed significant main effects of segment ($F_{3,585} = 33.74$, $p < 0.001$) and ROI ($F_{3,585} = 375.76$, $p < 0.001$) and a significant interaction ($F_{9,585} = 26.10$, $p < 0.001$). The interaction indicated that changes in similarity scores across segments differed across ROIs (Figure 2B). Considering each ROI separately, significant main effects of segment were observed in CA3/DG ($F_{3,177} = 5.15$, $p = 0.002$), PPA ($F_{3,117} = 28.71$, $p < 0.001$), and EVC ($F_{3,117} = 40.91$, $p < 0.001$) but not in CA1 ($F_{3,177} = 0.36$, $p = 0.783$). Whereas similarity scores in PPA and EVC robustly decreased across segments (paired samples t test of first vs. second half of the trial; PPA: $t_{39} = 7.21$, $p < 0.001$; EVC: $t_{39} = 8.64$, $p < 0.001$), similarity scores in CA3/DG significantly *increased* across time bins (first vs. second half: $t_{39} = -3.44$, $p = 0.001$) (for additional statistical comparisons, see Table S3). Thus, CA3/DG representations of overlapping routes were most distinct when the images were most similar. In fact, CA3/DG similarity scores were significantly below 0 during the first half of the trial (same + early-similar segment, one-sample t test: $t_{39} = -2.30$, $p = 0.027$). In other words, CA3/DG exhibited a repulsion effect (lower pattern similarity for overlapping routes than non-overlapping routes) that specifically occurred when the overlapping routes were identical or highly similar.

Within the similar segment alone, there were abrupt changes from the early-similar to late-similar segments in CA3/DG, PPA, and EVC. Again, however, these changes were in opposite directions. Whereas PPA/EVC similarity scores sharply decreased from the early-similar to late-similar segments (paired samples t tests; PPA: $t_{39} = 4.77$, $p < 0.001$; EVC: $t_{39} = 2.51$, $p = 0.016$), CA3/DG scores sharply *increased* from the early-similar to late-similar segments ($t_{39} = -3.81$, $p < 0.001$). CA3/DG scores were significantly below 0 in the early-similar segment ($t_{39} = -2.79$, $p = 0.008$) and significantly above 0 during the late-similar segment ($t_{39} = 2.08$,

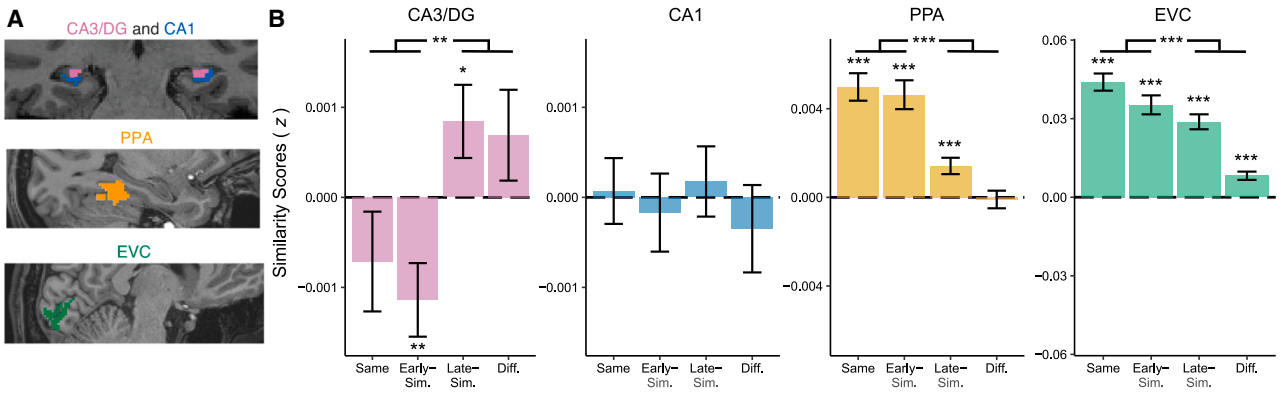

Figure 2. fMRI similarity scores as a function of route segment

(A) Regions of interest (ROIs) included hippocampal subfields CA3 and dentate gyrus (CA3/DG, pink), hippocampal subfield CA1 (blue), the parahippocampal place area (PPA, yellow), and early visual cortex (EVC, green). See Figure S2 for additional ROIs.

(B) Similarity scores were defined as the fMRI pattern similarity between overlapping routes relative to pattern similarity between non-overlapping routes. Positive similarity scores indicate that overlapping routes had more similar activity patterns than non-overlapping routes. Negative similarity scores indicate repulsion: that overlapping routes had less similar activity patterns than non-overlapping routes (see Figure S1 for a schematic illustration of repulsion). Within CA3/DG, similarity scores significantly increased from the first half of the route to the second half, with evidence of repulsion selective to the first half of the trial. By contrast, similarity scores significantly decreased from the first to second half of the trial in PPA and EVC, but with no evidence of repulsion. Asterisks above plots reflect paired samples t tests comparing first vs. second half (**$p < 0.01$, ***$p < 0.001$). Asterisks above/below bars reflect one-sample t tests comparing values to 0 (*$p < 0.05$, **$p < 0.01$, ***$p < 0.001$). Error bars are SEM. See Table S3 for additional statistics. See Figure S3 for alternative analysis.

$p = 0.045$). These changes in similarity scores within the similar segment parallel the behavioral data from post-tests 1 and 2, which indicated that discrimination of overlapping routes emerged during the similar segment (Table S2; Figure 1D).

Relationship between repulsion and MoI

We next sought to establish a direct link between CA3/DG repulsion and internal beliefs about a route's destination. We predicted that repulsion would be temporally coupled to the specific moment *within a trial* when participants were able to confidently disambiguate the overlapping routes. To test this, we used each participant's responses from post-test 2 to identify the exact time point when participants were highly confident (90% sure) of each route's destination. We refer to this critical time point as the MoI. Importantly, post-test 2 did not include probabilistic destination cues; thus, the data provide an independent measure of when participants were able to use subtle visual cues *within the route images* to determine the route destination. In other words, the MoI represents a threshold for route identification in the absence of destination cues. As in the preceding section, here we focus on fMRI data from valid trials.

To compute the MoI, for each participant we pooled the post-test 2 responses within each route pair. Pooling responses within a pair was necessary because the fMRI similarity scores were computed at the level of route pairs, not individual routes. The MoI for each pair was defined as the range (minimum to maximum) of the pooled responses. The mean duration of the MoI (i.e., the difference between the minimum and maximum) was 1.68 s, indicating that the MoI was a precise (narrow) temporal window relative to the full 24 s trial (Figure 3A). Time points prior to the MoI were defined as pre-MoI (mean length = 8.70 s), and time points after the MoI as post-MoI (mean length = 13.63 s) (Figure 3A).

CA3/DG similarity scores were significantly below 0 (repulsion effect) at the MoI (one-sample t test; $t_{39} = -3.32$, $p = 0.002$; Figure 3B) but did not differ from 0 pre-MoI ($t_{39} = -0.95$, $p = 0.350$) or post-MoI ($t_{39} = 1.24$, $p = 0.222$). Considering all three segments (pre-MoI, MoI, and post-MoI), there was a significant main effect of segment in CA3/DG (one-way ANOVA: $F_{2,78} = 5.74$, $p = 0.005$). This was primarily driven by a significant increase in similarity scores from the MoI to post-MoI segment (paired samples t test: $t_{39} = 3.28$, $p = 0.002$). There was no significant difference between pre-MoI and MoI ($t_{39} = -1.75$, $p = 0.088$). For CA1, EVC, and PPA, there was no evidence of repulsion effects at the MoI (all similarity scores were numerically positive). The main effect of segment was significant for EVC ($F_{2,78} = 30.79$, $p < 0.001$) and PPA ($F_{2,78} = 11.34$, $p < 0.001$) but not CA1 ($F_{2,78} = 0.69$, $p = 0.506$). However, in sharp contrast to CA3/DG, the main effects for EVC and PPA were driven by significant *decreases* in similarity scores from MoI to post-MoI (t_{39}'s > 3.44, p's < 0.001; Figure 3B). Thus, after participants gained insight into where the routes were headed, representations of overlapping routes became much less similar in EVC and PPA but much more similar in CA3/DG.

Finally, to confirm the temporal selectivity of the CA3/DG repulsion effect to the MoI, we performed a permutation test. For this analysis, similarity scores were computed for each participant, route pair, and time point within a route, as described above. The 24 time points were then shuffled (separately for each route pair and participant) before the MoI analysis proceeded. This process was repeated 10,000 times to obtain a distribution of permuted group-level mean similarity scores at the MoI. The actual (observed) mean similarity score at the MoI was lower than any of the 10,000 permuted means (i.e., $p < 0.0001$), clearly demonstrating that the repulsion effect at the MoI was stronger than what would be observed by randomly selecting time points within the routes. This strong temporal selectivity is notable given that the MoI was only measured after fMRI scanning. Taken together, these analyses demonstrate that repulsion was highly selective to CA3/DG and clearly

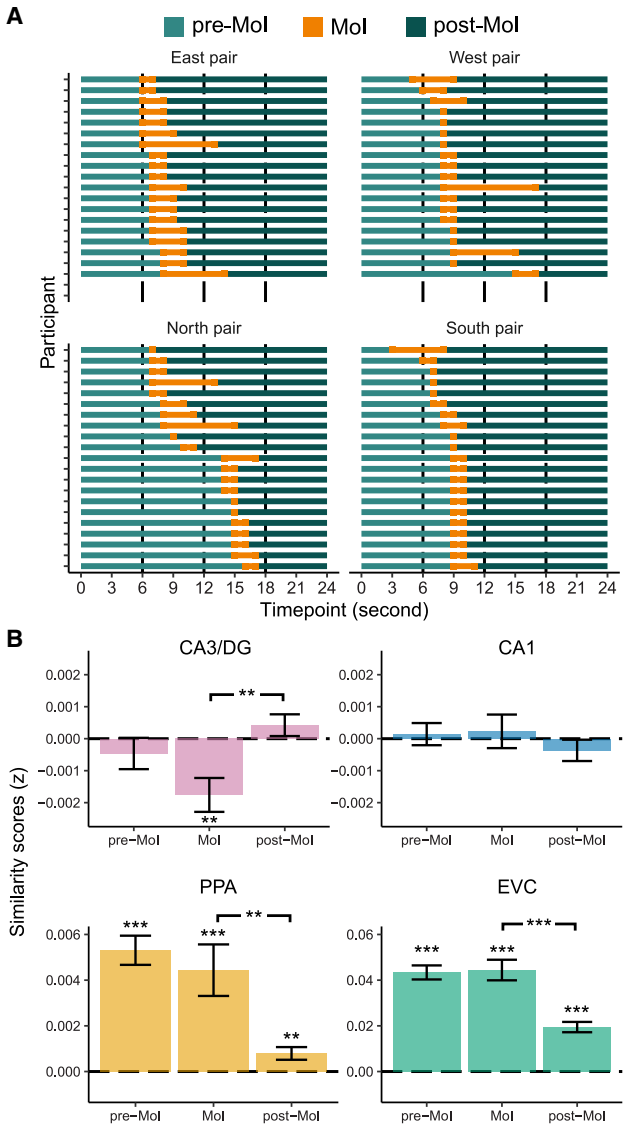

Figure 3. CA3/DG repulsion is temporally coupled to MoIs

(A) Distribution of moments of insight (MoIs) across route pairs and participants. Each participant studied two pairs of overlapping routes (east and west or south and north). For each participant and each pair of overlapping routes, the MoI was defined based on participants' responses during post-test 2 (responses indicated the moment at which participants were 90% sure of the destination). Within each of the four plots, each row corresponds to an individual participant. For visualization purposes, the rows (participants) are vertically rank-ordered within each plot by the timing of the MOI. The width of the MoI (orange bars) represents the range of responses (minimum to maximum).

(B) fMRI similarity scores at participant-specific MoI, as well as pre-MoI and post-MoI segments. For CA3/DG, a significant repulsion effect (similarity scores < 0) was observed at the MoI. Similarity scores in CA3/DG significantly increased from the MoI to post-MoI segment. In PPA and EVC, similarity scores showed an opposite pattern: significant decreases from the MoI to post-MoI segments. Asterisks above plots reflect paired samples t tests comparing segments (**$p < 0.01$, ***$p < 0.001$). Asterisks above/below bars reflect one-sample t tests comparing values to 0 (**$p < 0.01$, ***$p < 0.001$). Error bars are SEM.

time-locked to the moment when participants were able to internally disambiguate the overlapping routes.

Relationship between destination cues and repulsion

In a final set of analyses, we considered whether destination cues influenced CA3/DG repulsion. Notably, destination cues were only 75% valid, meaning that the beliefs generated by these cues may not have been as strong as the beliefs associated with the MoI. That said, given our overarching hypothesis that CA3/DG repulsion is driven by internal beliefs, we predicted that similarity scores in CA3/DG would be influenced by destination cues, even when fully controlling for sensory information.

In fMRI analyses presented thus far, pattern similarity between overlapping routes was computed using pairs of trials that were preceded by valid cues ("valid-valid" similarity scores). Here, we contrast valid-valid similarity scores with "valid-invalid" similarity scores (Figure 4A). For valid-invalid similarity scores, we again computed pattern similarity of overlapping routes relative to non-overlapping routes, but each pair of overlapping routes consisted of a validly cued route and an invalidly cued route. Thus, a trial where cue = X and destination = X (valid trial) would be correlated with a trial where cue = X and destination = Y (invalid trial). In terms of the actual route images that participants saw, there was absolutely no difference between a pair of valid-valid routes and a pair of valid-invalid routes. In both cases, the routes had the same, similar, and different segments, ending at distinct destinations. The only difference was that for the valid-valid routes, participants (correctly) *expected* the routes to end at distinct destinations (X vs. Y), whereas for the valid-invalid routes, participants (incorrectly) expected the routes to end at the same destination (X vs. X). We predicted that effects of destination cues on CA3/DG representations would be strongest during the early part of the trial—when visual information was most ambiguous.

As a first step, we compared the first half of each route (same + early-similar segments) to the second half (late-similar + different segments). For each ROI, we ran two-way ANOVAs with factors of half (1st and 2nd) and cue (valid-valid, valid-invalid). Within CA3/DG, there was a significant main effect of half ($F_{1,117}$ = 7.31, p = 0.008), reflecting an increase in similarity scores from the first to second half, but no main effect of cue ($F_{1,117}$ = 2.35, p = 0.128). However, there was a significant interaction between half and cue ($F_{1,117}$ = 4.39, p = 0.038; Figure 4B), driven by valid-valid similarity scores that were significantly lower than valid-invalid similarity scores in the first half of the trial (paired t test: t_{39} = −2.73, p = 0.009) but not in the second half of the trial (t_{39} = 0.45, p = 0.655). In EVC and PPA (but not CA1), there were significant main effects of half (PPA: $F_{1,117}$ = 131.85, $p < 0.001$; EVC: $F_{1,117}$ = 213.13, $p < 0.001$; CA1: $F_{1,117}$ = 0.53, p = 0.469), reflecting a decrease in similarity scores, but there were no main effects of cue or interactions between cue and half ($F_{1,117}$'s < 0.78, p's > 0.380; Figure 4B). When considering the first half of the trial alone, there was no difference between valid-valid and valid-invalid similarity scores for CA1, PPA, or EVC (t_{39}'s < 2.01, p's > 0.05). Thus, destination cues selectively influenced overlapping route representations within CA3/DG, particularly when visual information was most ambiguous.

We next conducted a time point-by-time point analysis of CA3/DG that specifically focused on the 6 time points during the same

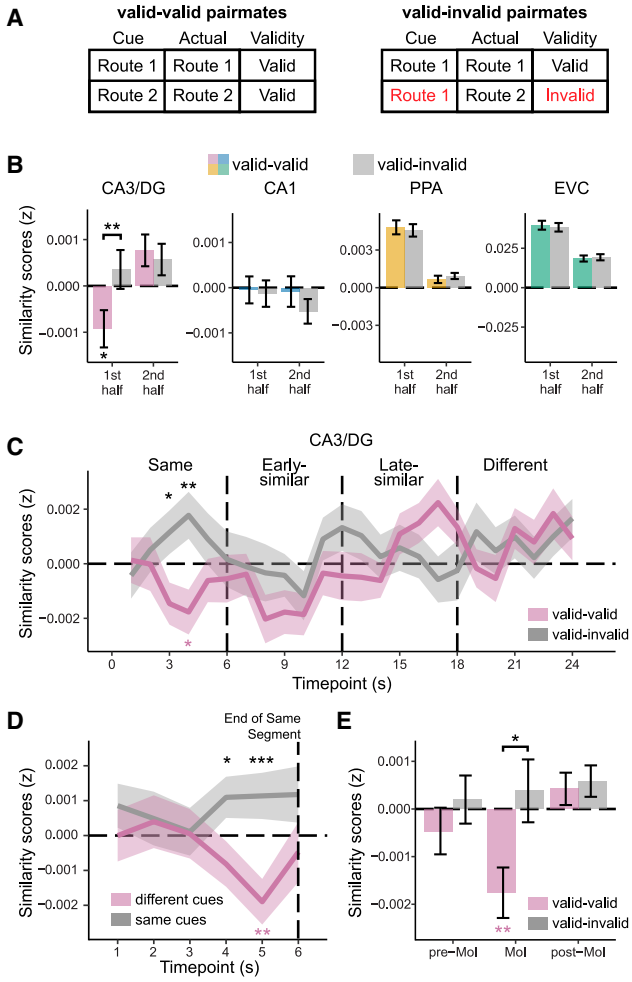

Figure 4. Influence of destination cues on similarity scores

(A) Schematic illustration of how valid-valid pairmates (left) and valid-invalid pairmates (right) were defined. In both cases, fMRI pattern similarity was computed between overlapping routes (e.g., routes 1 and 2). For valid-valid trials, cues accurately indicated that routes were headed to different destinations. For valid-invalid trials, cues were the same (e.g., "route 1"), but the destinations were different.

(B) fMRI similarity scores as a function of cues (valid-valid vs. valid-invalid) and route half (1st half of the route = picture index 1–50 vs. 2nd half of the route = picture index 51–100). Only CA3/DG showed a significant cue by half interaction (repeated measures two-way ANOVA, $p = 0.038$). For CA3/DG, within the first half, valid-valid similarity scores were significantly below 0 (repulsion effect; one-sample t test, $^{*}p = 0.027$) and significantly lower than valid-invalid similarity scores (paired samples t test, $^{**}p = 0.009$). Error bars are SEM.

(C) Time point-by-time point similarity scores in CA3/DG, separated by valid-valid and valid-invalid trials. Within the same segment (identical route images), similarity scores were significantly lower for valid-valid than valid-invalid trials at time points 3 and 4 (black asterisks, paired samples t tests, $^{*}p < 0.05$, $^{**}p < 0.01$). Valid-valid similarity scores were significantly below 0 (repulsion) at time point 4 (pink asterisk, one-sample t test, $^{*}p < 0.05$). Error bars are SEM.

(D) Alternate version of analysis in (C) that includes all pairs of trials for which participants viewed identical images during the same segment, with trials separated as a function of whether destination cues were the same ("same cue") or different ("different cue"). Similarity scores were significantly lower for different cue trials than same cue trials (black asterisks) at time points 4 and 5 (black asterisks, paired samples t tests, $^{*}p < 0.05$, $^{***}p < 0.001$). Similarity scores for different cue trials were significantly below 0 (pink asterisks) at time point 5 (one sample t test, $^{*}p < 0.01$). Error bars are SEM.

segment—when overlapping route images were identical. Thus, any effect of cues during the same segment can *only* be explained by the cues themselves. Again, we compared valid-valid to valid-invalid trials. All p values reported below are uncorrected for multiple comparisons; $p < 0.0083$ are significant at a Bonferroni-corrected threshold (i.e., $p < 0.05/6$ time points). Strikingly, valid-valid similarity scores were significantly lower than valid-invalid similarity scores at time point 4 ($t_{39} = -3.32$, $p = 0.002$; Figure 4C), with a similar effect at time point 3 ($t_{39} = -2.69$, $p = 0.010$). Qualitatively, the valid-valid and valid-invalid comparisons were mirror images of each other, with valid-valid similarity scores below 0 (repulsion; time point 3: $t_{39} = -1.89$, $p = 0.066$; time point 4: $t_{39} = -2.15$, $p = 0.038$) and valid-invalid similarity scores above 0. In an expanded version of this analysis, we pooled all trials that contained identical images during the same segment and split these trials according to whether the cues were the same vs. different (see STAR Methods). Again, we found that cues had a significant effect on CA3/DG similarity scores (Figure 4D). Namely, similarity scores were significantly lower when cues were different than when cues were the same (time point 4: $t_{39} = -2.47$, $p = 0.018$; time point 5: $t_{39} = -3.45$, $p = 0.001$). When the cues were different, similarity scores were significantly below 0 (repulsion) at time point 5 ($t_{39} = -2.90$, $p = 0.006$). Thus, when viewing *identical route images*, repulsion occurred—but only occurred—when internal beliefs were distinct.

Finally, we tested whether repulsion *at the MoI* was influenced by destination cues. We reasoned that valid destination cues could either potentiate repulsion at the MoI or, conversely, that repulsion at the MoI might be greater when internal beliefs were violated (invalid destination cues). To test this, we created three subject-specific MoI bins (pre-MoI, MoI, and post-MoI) and considered valid-valid trials (same data as Figure 3B) as well as valid-invalid trials. An ANOVA with factors of segment and cue revealed a significant main effect of cue ($F_{1,195} = 6.62$, $p = 0.011$), reflecting stronger repulsion in CA3/DG for valid-valid trials relative to valid-invalid trials. The main effect of segment was significant ($F_{2,195} = 3.23$, $p = 0.042$), as in the analysis restricted to valid-valid trials (Figure 3B). While the interaction between cue and segment was not significant ($F_{2,195} = 2.39$, $p = 0.094$), follow-up comparisons revealed that the cue effect was significant at the MoI ($t_{39} = -2.38$, $p = 0.022$) but not pre-MoI ($t_{39} = -1.06$, $p = 0.295$) or post-MoI ($t_{39} = -0.37$, $p = 0.712$).

Collectively, these analyses indicate that destination cues had an influence on CA3/DG similarity scores during the 1st half of the trial (Figure 4B), which was largely explained by two separate, transient effects: (1) an effect during the same segment that *preceded* the MoI (Figures 4C and 4D) and (2) an effect *at the MoI*, which, on average, occurred during the early-similar segment (Figure 4E). Thus, the influence of destination cues on CA3/DG repulsion was statistically dissociable from the effect of the MoI.

(E) CA3/DG similarity scores at pre-MoI, MoI, and post-MoI segments, separated for valid-valid trials (same data as Figure 3B) and valid-invalid trials. Similarity scores were significantly lower for valid-valid trials than valid-invalid trials overall (main effect of cue from two-way repeated measures ANOVA: $p = 0.011$) and at the MoI (black asterisk, paired samples t test, $^{*}p < 0.05$). At the MOI, valid-valid similarity scores were significantly below 0 (repulsion effect; pink asterisks, one sample t test, $^{**}p < .01$). Error bars are SEM.

DISCUSSION

Here, we show that representations of overlapping spatial routes in hippocampal subfields CA3 and DG (CA3/DG) exhibit a dramatic repulsion effect that specifically occurs when visual input to the hippocampus is highly similar—or even *identical*—but internal beliefs are distinct. In other words, high visual similarity and distinct internal beliefs are key ingredients for repulsion to occur, but it is the conjunction of these factors that powerfully drives CA3/DG representations apart.

The phenomenon of repulsion in the human hippocampus has now been reported several times.[6–14] By definition, repulsion refers to targeted differentiation of hippocampal activity patterns that is triggered by event similarity. However, we provide a unique and theory-driven test of the role of internal beliefs in repulsion. Our prediction that repulsion would be linked to internal beliefs was inspired by recent theoretical and empirical arguments that place cell remapping in rodents is better explained by internal beliefs than by external features of the environment.[24,25] That said, repulsion has not been reported in rodent place cells. In humans, there is evidence that internal beliefs about ambiguous stimuli are related to hippocampal activity patterns[31,32] but not specifically to repulsion. There is also evidence that repulsion is correlated with behavioral expressions of memory interference,[7,9,17] but this evidence does not uniquely favor an internal belief account.

Our first approach to linking hippocampal repulsion to internal beliefs involved using participant-specific subjective reports (collected after fMRI scanning) to identify the precise time point, within each route, when participants were "sure" of the route's destination (MoI). Because the MoI were based on participants' beliefs in the absence of probabilistic cues, they reflect the ability to discern the destination from subtle visual features. Notably, the MoI always occurred during the similar segment—that is, while the route images were still extremely similar (Figure 1). Despite this high visual similarity, the MoI were associated with robust repulsion, wherein CA3/DG representations of overlapping routes were *less similar* than representations of non-overlapping routes. Importantly, there was no evidence that similarity scores decreased in visual cortical areas at the MoI; instead, they only decreased *after* the MoI (Figure 3B). In fact, this was a mirror image of CA3/DG, where similarity scores *increased* after the MoI (Figure 3B). Thus, CA3/DG repulsion occurred (1) precisely when internal beliefs became distinct and (2) before there was any hint of differentiation within visual cortical areas.

Our second approach involved *manipulating* participants' internal beliefs while controlling for visual input. Specifically, during fMRI scanning, trials were preceded by probabilistic cues that indicated each route's likely destination. This allowed us to compare fMRI pattern similarity for overlapping routes when cues correctly indicated the routes were headed to distinct destinations (valid-valid pairs) vs. when cues incorrectly indicated the routes were headed to the same destination (valid-invalid pairs). In both cases, we were comparing route images that were initially identical (same segment) but terminated at distinct destinations. This manipulation revealed that, during the early portion of the route, CA3/DG repulsion depended on the *belief* that routes were headed to distinct destinations (Figure 4). In fact, when cues were distinct, repulsion was evident in CA3/DG before there were *any differences* in the route images (same segment; Figures 4C and 4D). Even at the MoI (when participants could potentially detect subtle differences in the routes), the influence of destination cues was still evident, with stronger repulsion in CA3/DG for valid-valid pairs (Figure 4E). Collectively, these results provide strong evidence that CA3/DG repulsion was related to internal beliefs, as opposed to CA3/DG inheriting or amplifying subtle differences in visual cortical input.

Importantly, the repulsion we observed in CA3/DG reflects a relationship between visual input similarity and neural similarity that violates standard models of pattern separation[1,2,18] (Figure S1). In particular, with "perfect orthogonalization," overlapping routes would be no more similar—but no less similar—than non-overlapping routes (similarity scores = 0). By contrast, we demonstrate instances where CA3/DG representations of overlapping routes were *less similar* than non-overlapping routes. Even if CA3/DG completely ignored visual input and, instead, only orthogonalized internal beliefs, this still "only" predicts that similarity scores would be equal to 0, not below 0. Thus, whether orthogonalization occurs at the level of visual input or at the level of internal beliefs, orthogonalization cannot explain our findings.[16,17]

Whereas orthogonalization involves statistical independence of representations, our findings suggest a *dependence* between overlapping route representations in CA3/DG. However, this dependence took the form of representations specifically *moving away from each other*. A helpful analogy is to consider a teacher that wishes to prevent a pair of students from talking during class. The teacher might move the students to opposite corners of the room. In this case, the teacher is not trying to maximize the distance between *all students* (the analog of orthogonalization) but instead maximizes the distance between the disruptive students (the analog of repulsion). Thus, the students end up being placed "far away" from each other precisely because of their initial proximity and interference.

The pattern of results we observed in CA3/DG also sharply contrasts with visual cortical areas—and these differences inform theoretical accounts of repulsion. For example, CA3/DG similarity scores were lowest (greatest repulsion) when similarity scores in the visual cortex were highest (Figure 2B). Once similarity scores in the visual cortex decreased (2nd half of trial), similarity scores in CA3/DG *increased* (repulsion disappeared). Our interpretation of these data is that the hippocampus is critically involved in differentiating events when sensory areas fail to do so. Once sensory representations are sufficiently distinct, the hippocampus is no longer needed and repulsion is not triggered. This trade-off can be conceptualized as a shift from internal to external representations. Because sensory evidence is ambiguous early in the trial, there is potentially greater reliance on competing internal representations (predictions) supported by the hippocampus.[33] Later, sensory evidence becomes less ambiguous and predictions are less important, shifting processing toward external representations encoded by the visual cortex. In fact, an interesting possibility is that repulsion of internal representations within the hippocampus early in the trial directly facilitates external visual attention later in the trial.[8]

While repulsion is not accounted for or predicted by many leading theories of memory and hippocampal function,[1,3,4,15]

the "non-monotonic plasticity hypothesis" has specifically been developed to account for repulsion-like effects in behavior and the brain.[13,34] According to this theory, repulsion reflects long-term plasticity that occurs when activation of a target memory spreads to similar, competing memories. In particular, when a competing memory is moderately activated, it is subject to synaptic weakening that reduces its connections to the target.[17,35,36] In the extreme, selective pruning of target-competitor connections can result in target-competitor similarity that is *lower* than similarity between unrelated events[17,34]—a repulsion effect. These changes are thought to be adaptive because they reduce memory interference in a very targeted manner.[17,37–39] Our findings strongly align with core predictions from this theory. However, a striking aspect of the current findings is that repulsion was highly dynamic and transient within a trial. This raises the question of whether the repulsion we observed necessarily required long-term plasticity.

An alternative possibility is that repulsion reflects dynamic lateral inhibition, without the need for long-term plasticity. Specifically, if similar events activate cells that feed into common inhibitory interneurons, then stronger activation of a target representation could directly and immediately inhibit the competitor representation via the shared inhibitory interneurons. One of the appeals of a lateral inhibition account is that it can explain why the repulsion effects tended to "peak" at particular time points. Namely, we observed a peak in the repulsion effect immediately after the cue (Figures 4C and 4D) and then again at the MoI (Figure 4E). In other words, whenever the target activation was (putatively) boosted, this may have increased lateral inhibition of the competitor. That said, while lateral inhibition is a core feature of models that explain competitive dynamics in the hippocampus,[40,41] these models have not explicitly referenced or attempted to explain repulsion.

The fact that we observed repulsion in CA3/DG, but not CA1, is consistent with evidence from human[9,11,14,15,21,42] and rodent studies[1–3,43] specifically implicating the CA3-DG circuit in disambiguating overlapping events. However, an interesting question is whether CA3 and the DG differentially contribute to repulsion? Although our scanning protocol did not allow us to confidently separate CA3 from the DG, evidence from rodent studies suggests potential distinctions between these subregions.[19,44] Whereas the DG is thought to perform relatively automatic pattern separation owing to sparse coding[45] and strong lateral inhibition,[40,41] CA3 exhibits attractor dynamics that allow for flexible changes between pattern completion and pattern separation processes.[3,19,46] CA3 representations are also thought to be less strictly dictated by sensory input. For example, CA3 supports recall of past experience,[47] anticipation of future experience,[48] and the interpretation of ambiguous sensory input.[49] Thus, our findings in CA3/DG align with many functions ascribed to these subregions. With more targeted fMRI protocols, it may be possible to tease apart and functionally dissociate the contributions of these subregions to repulsion.[13,20]

In summary, our findings demonstrate that representations of overlapping spatial routes in human CA3/DG exhibit dramatic repulsion effects when visual input is extremely similar (or even identical), but internal beliefs are distinct. By linking repulsion to internal beliefs, we provide insight into *when* and *why* this phenomenon occurs. These findings have important implications for theories of hippocampal function.[1–4] More broadly, by using a human fMRI paradigm that was inspired by rodent studies[28,29] and with predictions derived from properties of place cell remapping,[24,25] our approach and findings directly bridge the fields of human episodic memory and rodent spatial navigation.

RESOURCE AVAILABILITY

Lead contact

Further information and requests for resources should be directed to and will be fulfilled by the lead contact, Brice A. Kuhl (bkuhl@uoregon.edu).

Materials availability

This study did not generate new, unique reagents.

Data and code availability

- De-identified human fMRI and structural MRI data have been deposited at OpenNeuro as https://doi.org/10.18112/openneuro.ds005947.v1.0.0. They are publicly available as of the date of publication.
- De-identified human behavioral data and stimuli have been deposited through the Open Science Framework (OSF) as https://doi.org/10.17605/OSF.IO/HRFV7. They are publicly available as of the date of publication.
- All original code has been deposited at OSF and is publicly available at https://doi.org/10.17605/OSF.IO/HRFV7 as of the date of publication.
- Any additional information required to reanalyze the data reported in this paper is available from the lead contact upon request.

ACKNOWLEDGMENTS

This work was supported by NIH-NINDS 2R01NS089729 to B.A.K. and by NIH-NINDS F31NS126016 to G.W.

AUTHOR CONTRIBUTIONS

G.W., S.H., and B.A.K. designed the experiment. G.W. and S.H. recruited participants and collected data. G.W. and B.A.K. analyzed the data and wrote the manuscript.

DECLARATION OF INTERESTS

The authors declare no competing interests.

STAR★METHODS

Detailed methods are provided in the online version of this paper and include the following:

- KEY RESOURCES TABLE
- EXPERIMENTAL MODEL AND STUDY PARTICIPANT DETAILS
- METHOD DETAILS
  - Stimuli
  - Overview of experimental procedure
  - Experimental procedure prior to scanning
  - Experimental procedure during scanning
  - Experimental procedure after scanning
  - MRI acquisition
  - Anatomical data preprocessing
  - Functional data preprocessing
  - Regions of interest
- QUANTIFICATION AND STATISTICAL ANALYSES
  - fMRI measures of route similarity
  - Destination cue analyses
  - Moment of insight analysis
  - Statistical significance

SUPPLEMENTAL INFORMATION

Supplemental information can be found online at https://doi.org/10.1016/j.cub.2025.05.029.

Received: October 29, 2024
Revised: April 29, 2025
Accepted: May 12, 2025
Published: June 3, 2025

REFERENCES

1. Colgin, L.L., Moser, E.I., and Moser, M.-B. (2008). Understanding memory through hippocampal remapping. Trends Neurosci. *31*, 469–477. https://doi.org/10.1016/j.tins.2008.06.008.
2. Yassa, M.A., and Stark, C.E.L. (2011). Pattern separation in the hippocampus. Trends Neurosci. *34*, 515–525. https://doi.org/10.1016/j.tins.2011.06.006.
3. Rolls, E.T. (2013). The mechanisms for pattern completion and pattern separation in the hippocampus. Front. Syst. Neurosci. *7*, 74. https://doi.org/10.3389/fnsys.2013.00074.
4. O'Reilly, R.C., and McClelland, J.L. (1994). Hippocampal conjunctive encoding, storage, and recall: Avoiding a trade-off. Hippocampus *4*, 661–682. https://doi.org/10.1002/hipo.450040605.
5. O'Reilly, R.C., and Rudy, J.W. (2001). Conjunctive representations in learning and memory: Principles of cortical and hippocampal function. Psychol. Rev. *108*, 311–345. https://doi.org/10.1037/0033-295x.108.2.311.
6. Chanales, A.J.H., Oza, A., Favila, S.E., and Kuhl, B.A. (2017). Overlap among spatial memories triggers repulsion of hippocampal representations. Curr. Biol. *27*, 2307–2317.e5. https://doi.org/10.1016/j.cub.2017.06.057.
7. Favila, S.E., Chanales, A.J.H., and Kuhl, B.A. (2016). Experience-dependent hippocampal pattern differentiation prevents interference during subsequent learning. Nat. Commun. *7*, 11066. https://doi.org/10.1038/ncomms11066.
8. Favila, S.E., and Aly, M. (2023). Hippocampal mechanisms resolve competition in memory and perception. Preprint at bioRxiv. https://doi.org/10.1101/2023.10.09.561548.
9. Wanjia, G., Favila, S.E., Kim, G., Molitor, R.J., and Kuhl, B.A. (2021). Abrupt hippocampal remapping signals resolution of memory interference. Nat. Commun. *12*, 4816. https://doi.org/10.1038/s41467-021-25126-0.
10. Liu, C., Ye, Z., Chen, C., Axmacher, N., and Xue, G. (2022). Hippocampal representations of event structure and temporal context during episodic temporal order memory. Cereb. Cortex *32*, 1520–1534. https://doi.org/10.1093/cercor/bhab304.
11. Dimsdale-Zucker, H.R., Ritchey, M., Ekstrom, A.D., Yonelinas, A.P., and Ranganath, C. (2018). CA1 and CA3 differentially support spontaneous retrieval of episodic contexts within human hippocampal subfields. Nat. Commun. *9*, 294. https://doi.org/10.1038/s41467-017-02752-1.
12. Zheng, L., Gao, Z., McAvan, A.S., Isham, E.A., and Ekstrom, A.D. (2021). Partially overlapping spatial environments trigger reinstatement in hippocampus and schema representations in prefrontal cortex. Nat. Commun. *12*, 6231. https://doi.org/10.1038/s41467-021-26560-w.
13. Wammes, J., Norman, K.A., and Turk-Browne, N. (2022). Increasing stimulus similarity drives nonmonotonic representational change in hippocampus. eLife *11*, e68344. https://doi.org/10.7554/eLife.68344.
14. Kim, G., Norman, K.A., and Turk-Browne, N.B. (2017). Neural differentiation of incorrectly predicted memories. J. Neurosci. *37*, 2022–2031. https://doi.org/10.1523/JNEUROSCI.3272-16.2017.
15. Yassa, M.A., Lacy, J.W., Stark, S.M., Albert, M.S., Gallagher, M., and Stark, C.E.L. (2011). Pattern separation deficits associated with increased hippocampal CA3 and dentate gyrus activity in nondemented older adults. Hippocampus *21*, 968–979. https://doi.org/10.1002/hipo.20808.
16. Duncan, K.D., and Schlichting, M.L. (2018). Hippocampal representations as a function of time, subregion, and brain state. Neurobiol. Learn. Mem. *153*, 40–56. https://doi.org/10.1016/j.nlm.2018.03.006.
17. Hulbert, J.C., and Norman, K.A. (2015). Neural differentiation tracks improved recall of competing memories following interleaved study and retrieval practice. Cereb. Cortex *25*, 3994–4008. https://doi.org/10.1093/cercor/bhu284.
18. LaRocque, K.F., Smith, M.E., Carr, V.A., Witthoft, N., Grill-Spector, K., and Wagner, A.D. (2013). Global similarity and pattern separation in the human medial temporal lobe predict subsequent memory. J. Neurosci. *33*, 5466–5474. https://doi.org/10.1523/JNEUROSCI.4293-12.2013.
19. Knierim, J.J., and Neunuebel, J.P. (2016). Tracking the flow of hippocampal computation: Pattern separation, pattern completion, and attractor dynamics. Neurobiol. Learn. Mem. *129*, 38–49. https://doi.org/10.1016/j.nlm.2015.10.008.
20. Bein, O., and Davachi, L. (2024). Event integration and temporal differentiation: How hierarchical knowledge emerges in hippocampal subfields through learning. J. Neurosci. *44*, e0627232023. https://doi.org/10.1523/JNEUROSCI.0627-23.2023.
21. Molitor, R.J., Sherrill, K.R., Morton, N.W., Miller, A.A., and Preston, A.R. (2021). Memory reactivation during learning simultaneously promotes dentate gyrus/CA $_{2,3}$ pattern differentiation and CA $_{1}$ memory integration. J. Neurosci. *41*, 726–738. https://doi.org/10.1523/JNEUROSCI.0394-20.2020.
22. Schlichting, M.L., Mumford, J.A., and Preston, A.R. (2015). Learning-related representational changes reveal dissociable integration and separation signatures in the hippocampus and prefrontal cortex. Nat. Commun. *6*, 8151. https://doi.org/10.1038/ncomms9151.
23. Morton, N.W., Sherrill, K.R., and Preston, A.R. (2017). Memory integration constructs maps of space, time, and concepts. Curr. Opin. Behav. Sci. *17*, 161–168. https://doi.org/10.1016/j.cobeha.2017.08.007.
24. Sanders, H., Wilson, M.A., and Gershman, S.J. (2020). Hippocampal remapping as hidden state inference. eLife *9*, e51140. https://doi.org/10.7554/eLife.51140.
25. Keinath, A.T., Nieto-Posadas, A., Robinson, J.C., and Brandon, M.P. (2020). DG–CA3 circuitry mediates hippocampal representations of latent information. Nat. Commun. *11*, 3026. https://doi.org/10.1038/s41467-020-16825-1.
26. Pettit, N.L., Yuan, X.C., and Harvey, C.D. (2022). Hippocampal place codes are gated by behavioral engagement. Nat. Neurosci. *25*, 561–566. https://doi.org/10.1038/s41593-022-01050-4.
27. Benna, M.K., and Fusi, S. (2021). Place cells may simply be memory cells: Memory compression leads to spatial tuning and history dependence. Proc. Natl. Acad. Sci. USA *118*, e2018422118. https://doi.org/10.1073/pnas.2018422118.
28. Deacon, R.M.J., and Rawlins, J.N.P. (2006). T-maze alternation in the rodent. Nat. Protoc. *1*, 7–12. https://doi.org/10.1038/nprot.2006.2.
29. Wood, E.R., Dudchenko, P.A., Robitsek, R.J., and Eichenbaum, H. (2000). Hippocampal neurons encode information about different types of memory episodes occurring in the same location. Neuron *27*, 623–633. https://doi.org/10.1016/s0896-6273(00)00071-4.
30. Brown, T.I., Ross, R.S., Keller, J.B., Hasselmo, M.E., and Stern, C.E. (2010). Which way was I going? contextual retrieval supports the disambiguation of well learned overlapping navigational routes. J. Neurosci. *30*, 7414–7422. https://doi.org/10.1523/JNEUROSCI.6021-09.2010.
31. Julian, J.B., and Doeller, C.F. (2021). Remapping and realignment in the human hippocampal formation predict context-dependent spatial behavior. Nat. Neurosci. *24*, 863–872. https://doi.org/10.1038/s41593-021-00835-3.
32. Steemers, B., Vicente-Grabovetsky, A., Barry, C., Smulders, P., Schröder, T.N., Burgess, N., and Doeller, C.F. (2016). Hippocampal attractor

dynamics predict memory-based decision making. Curr. Biol. *26*, 1750–1757. https://doi.org/10.1016/j.cub.2016.04.063.

33. Lu, Q., Hasson, U., and Norman, K.A. (2022). A neural network model of when to retrieve and encode episodic memories. eLife *11*, e74445. https://doi.org/10.7554/eLife.74445.
34. Ritvo, V.J.H., Turk-Browne, N.B., and Norman, K.A. (2019). Nonmonotonic plasticity: How memory retrieval drives learning. Trends Cogn. Sci. *23*, 726–742. https://doi.org/10.1016/j.tics.2019.06.007.
35. Norman, K.A., Newman, E., Detre, G., and Polyn, S. (2006). How inhibitory oscillations can train neural networks and punish competitors. Neural Comput. *18*, 1577–1610. https://doi.org/10.1162/neco.2006.18.7.1577.
36. Norman, K.A., Newman, E.L., and Detre, G. (2007). A neural network model of retrieval-induced forgetting. Psychol. Rev. *114*, 887–953. https://doi.org/10.1037/0033-295X.114.4.887.
37. Chanales, A.J.H., Tremblay-McGaw, A.G., Drascher, M.L., and Kuhl, B.A. (2021). Adaptive repulsion of long-term memory representations is triggered by event similarity. Psychol. Sci. *32*, 705–720. https://doi.org/10.1177/0956797620972490.
38. Drascher, M.L., and Kuhl, B.A. (2022). Long-term memory interference is resolved via repulsion and precision along diagnostic memory dimensions. Psychon. Bull. Rev. *29*, 1898–1912. https://doi.org/10.3758/s13423-022-02082-4.
39. Zhao, Y., Chanales, A.J.H., and Kuhl, B.A. (2021). Adaptive memory distortions are predicted by feature representations in parietal cortex. J. Neurosci. *41*, 3014–3024. https://doi.org/10.1523/JNEUROSCI.2875-20.2021.
40. Miller, S.M., and Sahay, A. (2019). Functions of adult-born neurons in hippocampal memory interference and indexing. Nat. Neurosci. *22*, 1565–1575. https://doi.org/10.1038/s41593-019-0484-2.
41. Espinoza, C., Guzman, S.J., Zhang, X., and Jonas, P. (2018). Parvalbumin+ interneurons obey unique connectivity rules and establish a powerful lateral-inhibition microcircuit in dentate gyrus. Nat. Commun. *9*, 4605. https://doi.org/10.1038/s41467-018-06899-3.
42. Bakker, A., Kirwan, C.B., Miller, M., and Stark, C.E.L. (2008). Pattern separation in the human hippocampal CA3 and dentate gyrus. Science *319*, 1640–1642. https://doi.org/10.1126/science.1152882.
43. Knierim, J.J. (2015). The hippocampus. Curr. Biol. *25*, R1116–R1121. https://doi.org/10.1016/j.cub.2015.10.049.
44. Leutgeb, J.K., Leutgeb, S., Moser, M.-B., and Moser, E.I. (2007). Pattern separation in the dentate gyrus and CA3 of the hippocampus. Science *315*, 961–966. https://doi.org/10.1126/science.1135801.
45. Hainmueller, T., and Bartos, M. (2020). Dentate gyrus circuits for encoding, retrieval and discrimination of episodic memories. Nat. Rev. Neurosci. *21*, 153–168. https://doi.org/10.1038/s41583-019-0260-z.
46. Guzowski, J.F., Knierim, J.J., and Moser, E.I. (2004). Ensemble dynamics of hippocampal regions CA3 and CA1. Neuron *44*, 581–584. https://doi.org/10.1016/j.neuron.2004.11.003.
47. Nakazawa, K., Quirk, M.C., Chitwood, R.A., Watanabe, M., Yeckel, M.F., Sun, L.D., Kato, A., Carr, C.A., Johnston, D., Wilson, M.A., et al. (2002). Requirement for hippocampal CA3 NMDA receptors in associative memory recall. Science *297*, 211–218. https://doi.org/10.1126/science.1071795.
48. Johnson, A., and Redish, A.D. (2007). Neural ensembles in CA3 transiently encode paths forward of the animal at a decision point. J. Neurosci. *27*, 12176–12189. https://doi.org/10.1523/JNEUROSCI.3761-07.2007.
49. Kelemen, E., and Fenton, A.A. (2016). Coordinating different representations in the hippocampus. Neurobiol. Learn. Mem. *129*, 50–59. https://doi.org/10.1016/j.nlm.2015.12.011.
50. Wang, L., Mruczek, R.E.B., Arcaro, M.J., and Kastner, S. (2015). Probabilistic maps of visual topography in human cortex. Cereb. Cortex *25*, 3911–3931. https://doi.org/10.1093/cercor/bhu277.
51. Yarkoni, T., Poldrack, R.A., Nichols, T.E., Van Essen, D.C., and Wager, T. D. (2011). Large-scale automated synthesis of human functional neuroimaging data. Nat. Methods *8*, 665–670. https://doi.org/10.1038/nmeth.1635.
52. Yushkevich, P.A., Pluta, J.B., Wang, H., Xie, L., Ding, S.-L., Gertje, E. C., Mancuso, L., Kliot, D., Das, S.R., and Wolk, D.A. (2015). Automated volumetry and regional thickness analysis of hippocampal subfields and medial temporal cortical structures in mild cognitive impairment. Hum. Brain Mapp. *36*, 258–287. https://doi.org/10.1002/hbm.22627.

STAR★METHODS

KEY RESOURCES TABLE

REAGENT or RESOURCE	SOURCE	IDENTIFIER
Deposited data		
de-faced fMRI/MRI data	Generated by this study.	OpenNeuro: https://doi.org/10.18112/openneuro.ds005947.v1.0.0
Behavioral data and stimuli	Generated by this study.	OSF: https://doi.org/10.17605/OSF.IO/HRFV7
Software and algorithms		
fMRI Prep	https://fmriprep.org	RRID: SCR_016216
PsychoPy	http://www.psychopy.org	RRID: SCR_006571
R	http://www.r-project.org/	RRID: SCR_001905
ASHS	https://www.nitrc.org/projects/ashs	RRID: SCR_005996
Nipype	https://nipype.readthedocs.io/en/latest/index.html	RRID: SCR_002502
Nilearn	https://nilearn.github.io/stable/index.html	RRID: SCR_001362
Custom code	Generated by this study.	OSF: https://doi.org/10.17605/OSF.IO/HRFV7

EXPERIMENTAL MODEL AND STUDY PARTICIPANT DETAILS

A target sample size of 40 participants was determined in advance. To reach this sample size, forty-eight participants (27 female; mean age = 20.40 years, range = 18–32) were enrolled following procedures approved by the University of Oregon Institutional Review Board. Written informed consent was collected for each participant prior to the experiment. All participants were right-handed, native-English speakers with normal or corrected-to-normal vision, with no self-reported psychiatric or neurological disease. Three participants were excluded because they ended the experiment early (n = 2) or exited the scanner in the middle of the experiment (n = 1). Five participants were excluded because they failed to reach a pre-determined behavioral threshold (see 'experimental procedure after scanning' below, for details). All participants received monetary compensation for participating.

METHOD DETAILS

Stimuli

The stimuli consisted of eight routes, each corresponding to a stream of 100 images depicting a 'walk' through the University of Oregon campus. Images were screenshots taken from videos at a constant time interval. The videos were recorded from an egocentric perspective while a researcher walked along the route. All routes started at the same 4-way intersection on campus and ended at eight distinct destinations which were named after a visual object at the destination (e.g., 'pole' or 'window'). The 8 routes comprised 4 pairs of overlapping routes (Figure 1A). Each pair of overlapping routes left the starting intersection at a different cardinal direction (north, south, east, west). For each overlapping route pair, the first 25 images of the route were identical to each other. Thus, during this initial segment ('same segment'), it was impossible to distinguish overlapping routes from each other. The next 50 images were extremely similar, but not identical, across the overlapping routes ('similar' segment). Specifically, the images were taken from videos that travelled along the same path, but were recorded separately. Thus, images might differ in terms of people, bicycles, shadows, etc. For the last 25 images ('different segment'), the overlapping routes diverged (each route turned in an opposite direction) before reaching their respective destinations (Figures 1A and 1B). Each participant studied 2 pairs of routes (i.e., 4 routes). The assignment of routes was counterbalanced across participants such that each subject either studied the north/south routes or the east/west routes.

Overview of experimental procedure

The first part of the experiment took place in a testing room outside of the MRI scanner. In the testing room, informed consent was obtained and participants were given instructions for the full experiment. Then, participants completed a Learning phase (studying the routes) before entering the MRI scanner. Inside the scanner, participants first completed 2 rounds of a Practice phase (not scanned), which combined additional study and a Pre-Test. Then, participants completed 10 rounds of a Cue phase (scanned), which was the main experimental task. After exiting the scanner, participants completed two Post-Tests that assessed memory for the routes. The experiment was implemented in PsychoPy2021.2.3 and lasted ~3 hours, with ~2 hours inside the scanner.

Experimental procedure prior to scanning

During the Study phase, participants viewed each route 4 times in random order. On each trial, the 100 images for a given route were shown in succession. Each image appeared for 240 ms and was immediately followed by the next image. After all images from the route were shown (24 seconds), the destination for the route appeared (2000 ms). The destination was followed by a white fixation cross (3000 ms) and then the next trial started. No behavioral responses were required during this phase. Participants were instructed to pay careful attention to each route so that they would late be able to predict each route's destination.

During each round of the Pre-test phase (2 rounds, total), participants again viewed each route 4 times in random order. The timing of the image presentation in the Pre-test phase—and in all subsequent phases—was identical to the Study phase (i.e., 240 ms per image). For 3 of the 4 presentations, the trial was identical to the Study phase. However, the remaining presentation functioned as a test trial. On these test trials—which were unpredictable from the participants' perspective—the route paused once per segment (three pauses total per trial). At each pause, participants were shown all 4 possible destinations (distributed in a single row). The destination was only represented by a text label (e.g., 'pole'). Participants had a maximum of 4000 ms to select the correct destination for the current route by pressing one of four keys on a button box held in their right hand. If they answered within the allotted time, the words 'sure' and 'unsure' then appeared on the screen and participants had another 3000 ms (maximum) to respond using the button box to indicate their level of confidence. If participants did not respond within the allotted time for the initial set of four destinations, then the confidence decision was omitted. After the third pause/test, the trial continued to the destination. Pauses were restricted such that they only occurred at picture indices 10-25 for the same segment, 26-75 for the similar segment, and 76-90 for the different segment. Within these ranges, the actual pause was randomly determined on each trial. During the Pre-test phase (and the subsequent fMRI phase), stimuli were presented on a gray background, projected from the back of the scanner. Lights were turned off in the scanner room to ensure better contrast for the display.

Experimental procedure during scanning

In each round of the fMRI phase (10 rounds, total), participants viewed each route 4 times. Importantly, each trial was preceded by a text cue (1 s) indicating the likely destination (e.g., 'pole'). Cues were either *valid* (indicating the correct destination) or *invalid* (in which case the cue indicated the overlapping route's destination). Within each round of the fMRI phase, each route was preceded by a valid cue three times and by an invalid cue once. Thus, cues were 75% valid. However, one of the three valid trials served as a catch trial. Catch trials were identical in procedure and timing to the test trials in the Pre-test phase with the exceptions that catch trials (1) always paused (and only paused once) during the similar segment, (2) ended after the confidence rating (or after the destination selection timed out), (3) were preceded by a cue (which, again, was always valid), and (4) had slightly shorter response windows than Pre-Test trials (maximum of 3000 ms to select the destination and, if applicable, a maximum of 2000 ms for the confidence rating). Non-catch trials were always followed by a white fixation cross for 3000 ms before the start of the next trial. Catch trials were followed by a white fixation cross for 3000 ms + any time that was 'unused' for the destination selection and confidence ratings. In other words, the duration of the destination selection + confidence rating (if applicable) + fixation cross always summed to 8000 ms.

For catch trials, the pauses occurred randomly between picture indices 25 and 75, but with the constraint that the four catch trials within a given round were randomly divided into two yoked pairs such that the picture indices within each pair summed to 100. For example, if one catch trial was randomly determined to pause at picture index 65, then the yoked catch trial would pause at picture index 35. This constraint ensured that each fMRI scan was identical in length while still maintaining unpredictability about when routes would pause. Performance on the catch trials is difficult to interpret given that, by design, the trials were always preceded by valid cues. Instead, catch trials were intended to promote vigilance and to reinforce the validity of the cues. That said, participants selected the correct destination (which was also the cued destination) on 85.31% ± 11.04% of the catch trials. The correct destination was selected with high confidence on 69.13% ± 19.17% of the catch trials.

Experimental procedure after scanning

The first Post-test provided an explicit measure of participants' ability to discriminate between the overlapping routes (in the absence of any cues). Each trial was similar to the test trials from the Pre-test phase. Here, however, every trial contained four pauses (destination tests) that only occurred during the Similar Segment. The pauses occurred at picture indices 30, 45, 60, and 75. For participants 1–32, each route was tested twice in a random order; for participants 33-40, each route was tested 4 times (the difference across participants was due to a technical error in the computer script). An additional difference relative to the test trials from the Pre-test phase is that when pauses occurred during Post-test 1, participants saw a single display that only presented two destination options: the correct destination (target) and the destination of the overlapping route (competitor). Specifically, participants were given five response options, arranged in a single row, corresponding to "Definitely [Destination X]", "Probably [Destination X]", "Unsure", "Probably [Destination Y]", and "Definitely [Destination Y]." Participants used the trackpad on the laptop to select a response. There was no time limit for responses during this phase. After the pause/test at picture index 75, the trial ended. After a white fixation cross (3000 ms), the next trial started. Participants who were below 100% accuracy (regardless of confidence) at picture index 75 were excluded from the experiment (n = 5). The rationale for excluding these participants is that they did not demonstrate an ability to consistently differentiate the overlapping routes by the end of the similar segment (even after extensive training).

The second Post-test allowed participants to freely indicate the specific timepoint at which they were confident of the route's destination. As in Post-test 1, routes appeared 4 times each in random order (again without cues). Each trial started with the presentation of the first image (picture index 1) followed by subsequent images up until participants made a response (using the keyboard) to

indicate that they were '90% sure' of the route's destination. Upon making a button press, the route image was replaced by the four destination labels. Participants used the keyboard to select the destination for the route. After a response was made, a white fixation cross appeared for 3000 ms and then the next trial began. There was no time limit for responses during this phase.

MRI acquisition

All images were acquired on a Siemens 3T Prisma MRI system in the Lewis Center for Neuroimaging at the University of Oregon. Functional data were acquired with a T2*-weighted echo-planar imaging sequence with partial brain coverage that prioritized full coverage of the hippocampus and early visual cortex (repetition time = 1000 ms, echo time = 33 ms, flip angle = 55°, 66 slices, 1.7 × 1.7 × 1.7 mm voxels). A total of 10 functional scans were acquired. Each functional scan comprised 458 volumes and included 6 s of lead-in time and 6 s of lead-out time at the beginning and end of each scan, respectively. Anatomical scans included a whole-brain high-resolution T1-weighted magnetization prepared rapid acquisition gradient-echo anatomical volume (1 × 1 × 1 mm voxels) and a high-resolution (coronal direction) T2-weighted scan (0.43 × 0.43 × 1.8 mm voxels) to facilitate segmentation of hippocampal subfields.

Anatomical data preprocessing

Preprocessing was performed using *fMRIPrep* 21.0.1 (RRID:SCR_016216), which is based on *Nipype* 1.6.1 (RRID:SCR_002502). The T1-weighted (T1w) image was corrected for intensity nonuniformity (INU) with N4BiasFieldCorrection54 (ANTs 2.3.3, RRID: SCR_004757), and used as the T1w reference throughout the workflow. The T1w reference was skull-stripped with the antsBrainExtraction.sh workflow (ANTs) in Nipype, using OASIS30ANTs as the target template. Brain tissue segmentation of cerebrospinal fluid (CSF), white-matter (WM), and gray-matter (GM) was performed on the brain-extracted T1w using FAST (FSL 6.0.5.1:57b01774, RRID:SCR_002823). Brain surfaces were reconstructed using recon-all (FreeSurfer 6.0.1, RRID:SCR_001847). Volume-based spatial normalization to one standard space (MNI152NLin2009cAsym) was performed through nonlinear registration with antsRegistration (ANTs 2.3.3), using brain-extracted versions of both T1w reference and the T1w template. *ICBM 152 Nonlinear Asymmetrical template version 2009c* was selected for spatial normalization (RRID:SCR_008796; TemplateFlow ID: MNI152NLin2009cAsym).

Functional data preprocessing

For each participant, a reference volume and its skullstripped version were generated for each of the 10 scan runs by aligning and averaging a single-band reference. For each participant, a fieldmap was collected and estimated based on two echo-planar imaging (EPI) references with topup (FSL 6.0.5.1:57b01774). The estimated fieldmap was then aligned with rigid-registration to the target EPI reference run and the field coefficients were mapped on to the reference EPI. Each scan run was slice-time corrected to 0.445s (0.5 of slice acquisition range 0s-0.89s) using 3dTshift from AFNI (RRID:SCR_005927). The single-band reference was then co-registered to the T1w reference using bbregister (FreeSurfer). Several potentially confounding variables were computed, including: framewise displacement (FD), DVARS, and three region-wise global signals. Additionally, a set of physiological regressors were extracted to allow for component-based noise correction (CompCor). Principal components were estimated after high-pass filtering the preprocessed BOLD time-series (using a discrete cosine filter with 128 s cut-off) for the anatomical CompCor variants (aCompCor). Frames that exceeded a threshold of 0.5 mm FD or 1.5 standardized DVARS were annotated as motion outliers.

The first 6 volumes of each scan run (lead-in time) were discarded. Then, 10 brain masks were generated by fMRIPrep for each of the 10 functional scans. The intersection of all 10 masks was used to perform brain extraction. For each scan run, each voxel was scaled at a mean equal to 100, with an upper bound of 200 and a lower bound of 0. A high-pass filter of 128 seconds was applied to each scan run. Separate categorical regressors were generated to indicate volumes more than 3 standard deviations above or below the global mean or volumes with FD higher than 0.5 mm. To control for nuisance variables, for each scan run a GLM was then applied that included these two categorical regressors along with FD, xyz translation, xyz rotation, aCompCor00-05, and the mean CSF value. Finally, in order to reduce noise in the timeseries data, temporal smoothing was applied within each scan such that, for each voxel, the BOLD response at each TR (volume n) was replaced by the average of the response at volumes n-1, n, and n+1.

Regions of interest

A region of interest (ROI) for early visual cortex (EVC) was created from the probabilistic maps of Visual Topography63[50] in MNI space with a 0.5 threshold. This ROI was transformed into each participant's native space using inverse T1w-to-MNI nonlinear transformation. For each participant, an ROI for PPA was created by first using Neurosynth[51] to perform a meta-analysis with the keyword ''place''. Results of the meta-analysis were thresholded by a z-score > 2 using the ''associative test'' option in Neurosynth. We visually inspected the whole-brain results and manually selected the two largest clusters that were spatially consistent with PPA. One cluster was in the right hemisphere (247 voxels) and one cluster was in the left hemisphere (163 voxels). These clusters were combined into a single PPA mask. This mask was then transformed into each participant's native space using the inverse T1w-to-MNI transformation. To create hippocampal ROIs, we used the Automatic Segmentation of Hippocampal Subfields (ASHS) 64 toolbox[52] with the upenn2017 atlas. This generated subfield ROIs in each participant's hippocampal body, including CA3/DG (which included CA2, CA3, and dentate gyrus) and CA1. The most anterior and posterior slices of the hippocampal body were manually determined for each participant based on the T2-weighted anatomical image. Each participant's subfield segmentations were also manually inspected to ensure the accuracy of the segmentation protocol. Then, each subfield ROI was transformed from the T2 space into the T1

space using the T2-to-T1w transformation, calculated with FLIRT (fsl) with six degrees of freedom, implemented with Nipype. All ROIs were again visually inspected following the transformation to T1 space to ensure the ROIs were anatomically correct.

QUANTIFICATION AND STATISTICAL ANALYSES

fMRI measures of route similarity

fMRI pattern similarity analyses were used to compute the degree of similarity between overlapping routes relative to non-overlapping routes. All pattern similarity analyses (correlations) were computed between trials from *different scan runs* (correlations were never performed within a scan run). The rationale for restricting correlations to trials from different scan runs was to control for autocorrelation within scan runs that can dramatically inflate similarity between trials that are nearby in time. To account for hemodynamic response lag, the temporally-smoothed fMRI timeseries for each voxel was first shifted by 6 s, such that the first *timepoint* within each trial was defined as the 6^{th} volume relative to the onset of the route images (each TR = 1 s). Pattern similarity analyses were then performed, separately for each of the 24 timepoints, by computing Pearson correlations For example, timepoint 1 from trial 1 in scan 1 would be correlated with timepoint 1 from trial 1 in scan 2, timepoint 1 from trial 2 in scan 2, all the way through timepoint 1 from the last trial in scan 10. Catch trials were excluded from pattern similarity analyses. All pattern similarity analyses were performed in participants' native space and correlation coefficients were Fisher z-transformed before any averaging (hereinafter referred to as pattern similarity).

Of central interest was the similarity between overlapping routes *relative* to the similarity between non-overlapping routes. Specifically, for each participant and each pair of overlapping routes, the mean pattern similarity between non-overlapping routes was subtracted from the mean pattern similarity between the overlapping routes, yielding a *similarity score*. For initial analyses, similarity scores were restricted to trials with valid cues, meaning that pattern similarity was always computed between pairs of trials (whether pairs of overlapping routes or pairs of non-overlapping routes) for which each route was preceded by a valid destination cue ('valid-valid' similarity scores).

Although similarity scores were always computed separately for each timepoint in a route (24 timepoints per route), we report many of the analyses as a function of route segment (same, early-similar, late-similar, different) instead of route timepoint. In these cases, we simply averaged similarity scores across the timepoints within each segment (e.g., an average of the 6 similarity scores within the same segment).

Destination cue analyses

In order to test for an influence of cue validity, we separately computed 'valid-invalid' similarity scores. As with valid-valid similarity scores, the valid-invalid similarity scores were computed by subtracting mean pattern similarity between non-overlapping routes from the mean pattern similarity between overlapping routes. However, valid-invalid similarity scores were based on pattern similarity between pairs of trials (whether pairs of overlapping routes or pairs of non-overlapping routes) for which one route was preceded by a valid cue and the other route was preceded by an invalid cue. It is important to emphasize that, in terms of the actual *route images* that participants saw there was no distinction between valid-valid overlapping routes versus valid-invalid overlapping routes. In other words, whether route 1 was preceded by a valid cue or an invalid cue, and whether route 2 was preceded by a valid cue or an invalid cue had no bearing on the route images participants saw—these overlapping routes always had same, similar and different segments and terminated at distinct destinations. However, in the specific case when one of the cues was valid *and* the other cue was invalid, then participants were led to believe that the two routes were headed to the same destination. For example, if the route 1 cue was valid and the route 2 cue was invalid, then both trials would be preceded by a cue indicating the route 1 destination (because invalid cues always referred to the destination of the overlapping route).

In an alternate analysis, we tested the effect of destination cues—specifically focusing on the same segment—by computing similarity scores using *all pairs* of trials for which participants viewed identical images during the same segment and separating these trials as a function of whether the cues were the same ('same cue') or different ('different cue'). The rationale for this alternate analysis, the results of which are shown in Figure 4D, is that it allowed for inclusion of more data because we now included correlations between pairs of identical routes (e.g., similarity between two separate route 1 trials). Similarity scores were computed following the same steps and rules described above (including baselining against non-overlapping route similarity), with the only differences being that: 'Same cue' data included (1) correlations between pairs of trials depicting the exact same route, validly cued each time, (2) correlations between pairs of trials depicting the exact same route, invalidly cued each time, and (3) correlations between pairs of overlapping routes, validly cued for one route and invalidly cued for the other route (i.e., valid-invalid trials, as described above); 'Different cue' data included (1) correlations between pairs of trials depicting the exact same route, validly cued for one route and invalidly cued for the other route, (2) correlations between pairs of overlapping routes, validly cued for both routes (i.e., valid-valid trials, as described in the main text), and (3) correlations between pairs of overlapping routes, invalidly cued for both routes.

Moment of insight analysis

Behavioral responses from Post-test 2 were used to identify the specific point in time at which participants were confident (''90% sure'') about each route's destination. We refer to this as the moment of insight (MoI). For each participant, each route was tested 4 times in Post-test 2. For each pair of overlapping routes (8 total trials), we pooled all responses and defined the MoI as the range of these response (minimum to maximum, rounded to nearest whole numbers). The rationale for pooling across overlapping routes

(as opposed to generating a separate MoI for each route) was that fMRI similarity scores for overlapping routes necessarily reflected the relative similarity or a *pair* of overlapping routes. Thus, it was preferable for the MoI to also be at the level of overlapping route pairs. All timepoints prior to the MoI are referred to as pre-MoI and all timepoints after the MoI are referred to as post-MoI. As with other analyses that were based on route segments (see above), similarity scores were first computed at individual timepoints and then similarity scores were averaged across all timepoints within the pre-MoI, MoI and post-MoI segments.

Statistical significance

For all statistical analyses (t-tests, ANOVA, permutation tests), a threshold of $p < .05$ was used to establish statistical significance. All t tests were two-tailed. All ANOVAs were calculated using linear mixed effects models, implemented with lme4 and lmerTest package in R, with random intercepts for participants. Degrees of freedom were approximated (as part of the lmerTest package) using the Satterthwaite method.